LBL-19816
Preprint c.2

Lawrence Berkeley Laboratory

UNIVERSITY OF CALIFORNIA

RECEIVED
LIBRARY
OCT 10 1985
LIBRARY AND
DOCUMENTS SECTION

Materials & Molecular Research Division

Submitted to the Journal of the
Electrochemical Society

ANODIC DISSOLUTION OF IRON IN ACIDIC SULFATE ELECTROLYTES. PART I: FORMATION AND GROWTH OF A POROUS SALT FILM

P. Russell and J. Newman

June 1985

TWO-WEEK LOAN COPY
This is a Library Circulating Copy
which may be borrowed for two weeks.

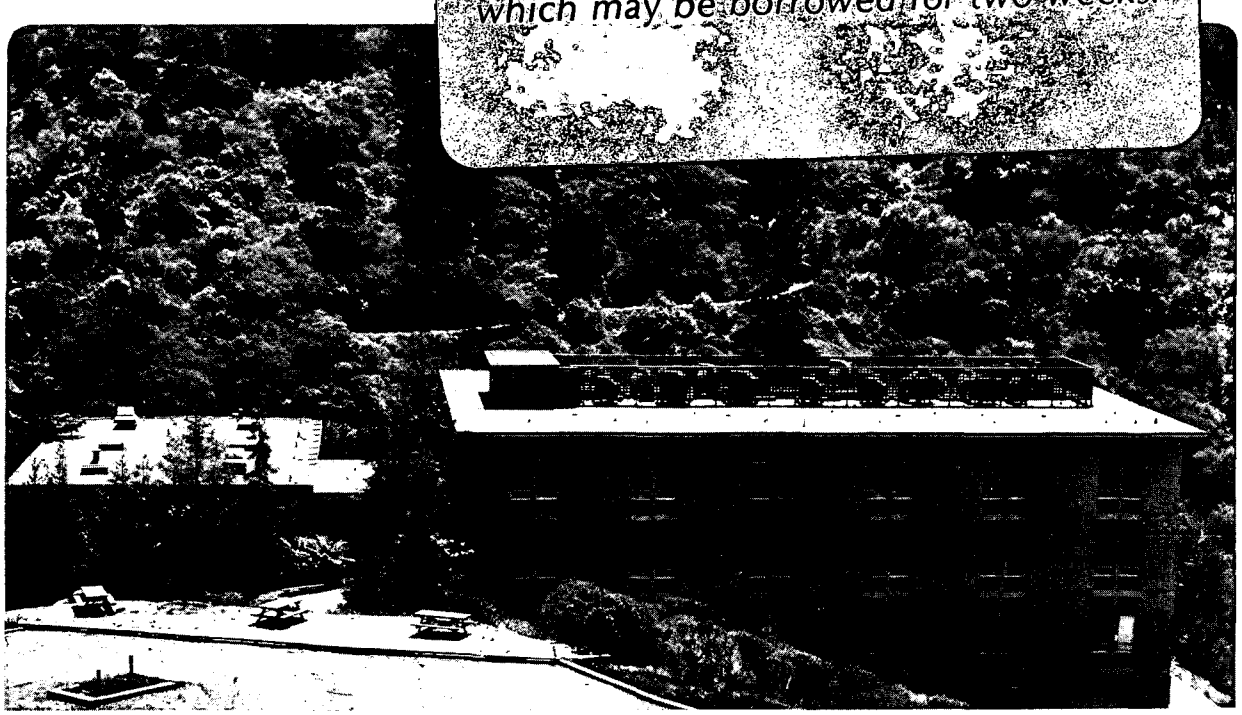

LBL-19816 c.2

Prepared for the U.S. Department of Energy under Contract DE-AC03-76SF00098

DISCLAIMER

This document was prepared as an account of work sponsored by the United States Government. While this document is believed to contain correct information, neither the United States Government nor any agency thereof, nor the Regents of the University of California, nor any of their employees, makes any warranty, express or implied, or assumes any legal responsibility for the accuracy, completeness, or usefulness of any information, apparatus, product, or process disclosed, or represents that its use would not infringe privately owned rights. Reference herein to any specific commercial product, process, or service by its trade name, trademark, manufacturer, or otherwise, does not necessarily constitute or imply its endorsement, recommendation, or favoring by the United States Government or any agency thereof, or the Regents of the University of California. The views and opinions of authors expressed herein do not necessarily state or reflect those of the United States Government or any agency thereof or the Regents of the University of California.

LBL—19816

Anodic Dissolution of Iron in Acidic Sulfate Electrolytes

Part I: Formation and Growth of a Porous Salt Film

Philip Russell[1,*] and John Newman[*]

Materials and Molecular Research Division,
Lawrence Berkeley Laboratory, and
Department of Chemical Engineering,
University of California, Berkeley, California 94720

June, 1985

Abstract

High-rate anodic dissolution of iron in a sulfuric acid electrolyte causes the solution near the electrode surface to become supersaturated in ferrous sulfate. Ferrous sulfate crystals precipitate on the electrode surface when the surface concentration exceeds a critical value. This critical value is about 1.8 times greater than the saturation concentration of ferrous sulfate. Continued precipitation results in the growth of a porous ferrous sulfate film on the surface. A mathematical model describing the initial formation and subsequent growth of this salt film is developed. A perturbation analysis serves as the foundation of this model. The salt-film thickness is nearly proportional to the square root of time shortly after the initial precipitation. The film growth rate falls off sharply in time following this initial period because of depletion of ferrous ions from the solution adjacent to the electrode surface.

---

[1]Present address: Weyerhaeuser Technology Center, Tacoma, Washington 98477

[*]Electrochemical Society Active Member

Key words: surface, corrosion, precipitation

This paper describes the processes that lead to formation of a porous salt film on an iron electrode surface. It is assumed that the current oscillations observed during anodic polarization of iron in acidic sulfate solutions[1,2] are caused by transitions between the active and the passive states. Beck[3] has demonstrated that formation of a salt film composed of ferrous sulfate is a necessary precursor to oxide passivation for iron in sulfuric acid solutions. Other authors have also shown the importance of salt-film formation in the passivation of iron,[4] particularly in the presence of convection.[5] This paper describes the buildup of ferrous ions near the electrode surface that leads to the initial precipitation and growth of the salt film. These processes are mathematically modeled. A perturbation technique is used as a guide in setting up the equations describing initial film formation. The perturbation solution indicates sources of errors in the numerical formulation and may be used to estimate the order of magnitude of these errors.

We now describe the events that lead to film formation. Initially, no salt film covers the electrode surface. Assume that the electrode potential is stepped from the open-circuit potential to a value where a limiting current or sustained current oscillations are observed. A high current begins to flow. The ferrous ion concentration builds up in the diffusion layer near the electrode surface. The surface concentration transiently increases above the saturation concentration of $FeSO_4$ to a maximum supersaturation value. The maximum supersaturation concentration is between 1.8 and 2.6 times greater than the saturation value.[3]

Ferrous sulfate crystals precipitate on the electrode surface when the ferrous ion concentration reaches this maximum value. The surface concentration instantly decreases to the saturation concentration. This process is depicted in Figure 1. The light line indicates the ferrous

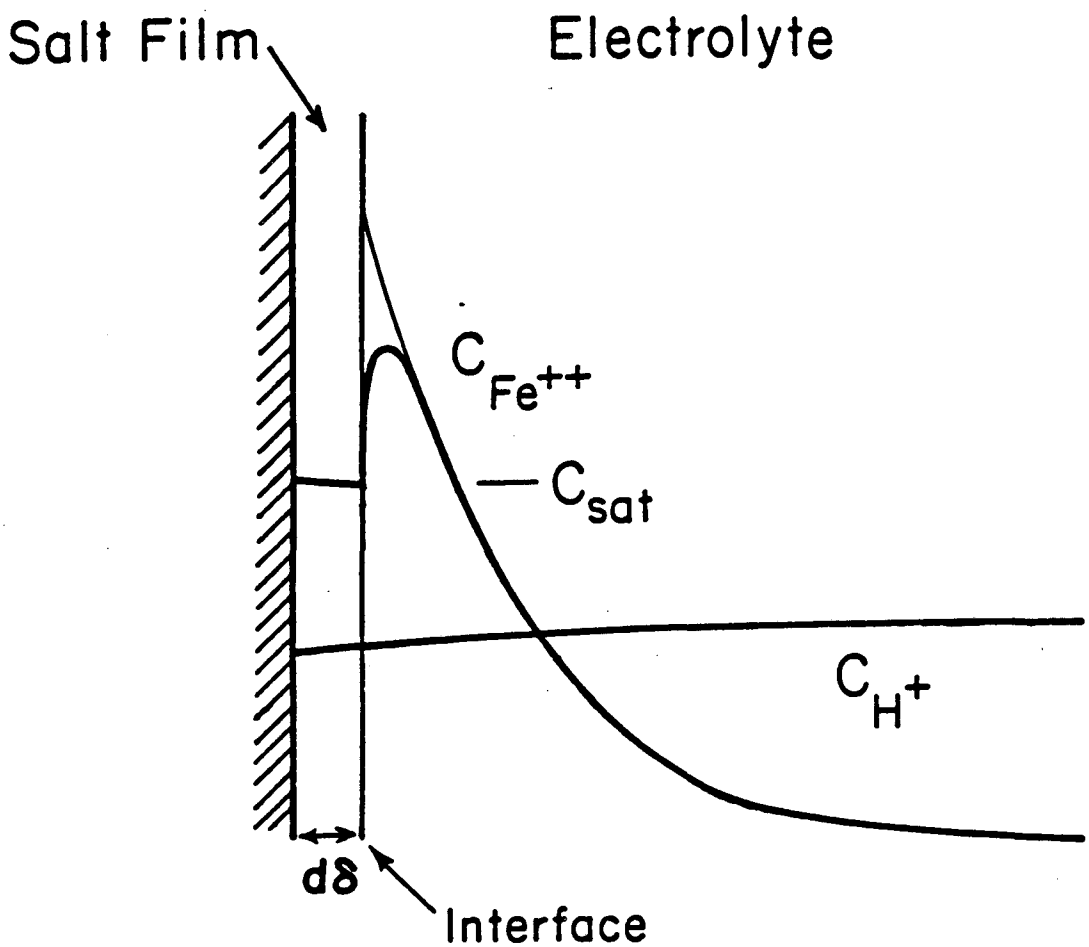

Figure 1. The concentration profile of ferrous and hydrogen ions a short time after the beginning of precipitation.

concentration just prior to precipitation. The heavy line is the profile a short time after initial precipitation. The steep concentration gradient results in a flux of ferrous ions that provides material for salt-film formation. The salt film has grown to a thickness of $d\delta$ in this short time dt.

Mathematical model

The equations that describe the ferrous ion concentration buildup process will be derived in this section. This concentration buildup, when no salt film is present, will be referred to as phase 1. Four ionic species and the potential are included in this model. The unknowns are numbered in the following way for notational convenience:

1	HSO_4^-	2	H^+
3	SO_4^{--}	4	Fe^{++}
5	Φ		

The concentration of each ionic species is governed by the following material balance equation.

$$\frac{\partial c_i}{\partial t} = -\nabla\cdot\mathbf{N}_i + R_i \,. \tag{1}$$

The flux density, $\mathbf{N}_i$, contains contributions due to migration, diffusion, and convection:

$$\mathbf{N}_i = -z_i u_i F c_i \nabla\Phi - D_i \nabla c_i + \mathbf{v} c_i \,. \tag{2}$$

The current may be calculated at any position by summing the charge that is being transported by the individual species.

$$\mathbf{i} = F \sum_i z_i \mathbf{N}_i \,. \tag{3}$$

The solution is assumed to be electrically neutral.

$$\sum_i z_i c_i = 0 \,. \tag{4}$$

Equations (1), with i = 1 to 4, along with Equation (4) are sufficient to solve for the five unknowns listed above.

The bisulfate, sulfate, and hydrogen ions may undergo the following homogeneous reaction

$$HSO_4^- = H^+ + SO_4^{--} . \tag{5}$$

It is assumed that rapid equilibrium exists and that it is governed by[6]

$$K = \frac{c_2 c_3}{c_1} . \tag{6}$$

Equation (5) indicates that $R_1 = -R_2$. Addition of the material balance Equation (1) for the bisulfate species (i = 1) to that of the hydrogen species (i = 2) results in a combination equation that no longer contains the homogeneous reaction term explicitly.[7,8]

$$\sum_{i=1}^{2} \frac{\partial c_i}{\partial t^*} = -\sum_{i=1}^{2} \nabla \cdot \mathbf{N}_i . \tag{7}$$

Equations (6) and (7) replace Equations (1) for i = 1 and 2.

Conservation of charge implies that the current density must be independent of position in a one-dimensional system.

$$\nabla \cdot \mathbf{i} = F \sum_{i=1}^{4} z_i \nabla \cdot \mathbf{N}_i = 0 . \tag{8}$$

Equation (8) may replace Equation (1) for i = 3.

Equations (4), (6) to (8), and Equation (1) with i = 4 are the five independent equations used to solve for the concentrations of the four ionic species and the potential. R_4 is assumed to be equal to zero in Equation (1).

One-dimensional form

This model considers variations only in the direction normal to the electrode surface, y. Radial variations are ignored. In the following development, the velocity in the electrolyte is approximated by the first term of its power-series expansion in y:[9,10]

$$v_y = -a\Omega\left(\frac{\Omega}{\nu}\right)^{1/2} y^2 , \tag{9}$$

where $a = 0.51023$. A dimensionless time[11] and distance[12] are defined as

$$t = \Omega\left(\frac{D_4}{\nu}\right)^{1/3}\left(\frac{a}{3}\right)^{2/3} t^* , \tag{10}$$

and

$$x = \left(\frac{a\,\nu}{3\,D_4}\right)^{1/3}\left(\frac{\Omega}{\nu}\right)^{1/2} y . \tag{11}$$

In terms of these dimensionless variables, Equation (7) becomes

$$\sum_{i=1}^{2}\left(\frac{\partial c_i}{\partial t}\right)_x = \sum_{i=1}^{2}\left\{\frac{z_i u_i F}{D_4}\frac{\partial}{\partial x}\left(c_i\frac{\partial \Phi}{\partial x}\right) + 3x^2\frac{\partial c_i}{\partial x} + \frac{D_i}{D_4}\frac{\partial^2 c_i}{\partial x^2}\right\}. \tag{12}$$

The material balance for Fe^{++}, Equation (1) with $i = 4$, becomes

$$\left(\frac{\partial c_4}{\partial t}\right)_x = \frac{z_4 u_4 F}{D_4}\frac{\partial}{\partial x}\left(c_4\frac{\partial \Phi}{\partial x}\right) + 3x^2\frac{\partial c_4}{\partial x} + \frac{\partial^2 c_4}{\partial x^2} . \tag{13}$$

Equation (8) becomes

$$-F^2\frac{\partial}{\partial x}\left(\frac{\partial \Phi}{\partial x}\sum_{i=1}^{4} z_i^2 u_i c_i\right) - F\sum_{i=1}^{4} z_i D_i\frac{\partial^2 c_i}{\partial x^2} = 0 . \tag{14}$$

The concentration buildup of ferrous ions is a transient process. The following distance variable permits more accurate monitoring of this process because it is stretched by the square root of time.

$$\xi = x/\sqrt{t} . \tag{15}$$

The time derivatives of concentration in the preceding material balance equations should be evaluated at constant x. The following transformation gives the relationship between time derivatives at constant x and constant ξ.

$$\begin{aligned}\left(\frac{\partial c_i}{\partial t}\right)_x &= \left(\frac{\partial c_i}{\partial t}\right)_\xi\left(\frac{\partial t}{\partial t}\right)_x + \left(\frac{\partial c_i}{\partial \xi}\right)_t\left(\frac{\partial \xi}{\partial t}\right)_x \\ &= \left(\frac{\partial c_i}{\partial t}\right)_\xi - \frac{\xi}{2t}\left(\frac{\partial c_i}{\partial \xi}\right)_t .\end{aligned} \tag{16}$$

Substitution of this transformation into Equations (12) to (14) gives

$$t \sum_{i=1}^{2} \left(\frac{\partial c_i}{\partial t}\right)_\xi = \sum_{i=1}^{2} \left\{ \frac{\xi}{2} \frac{\partial c_i}{\partial \xi} + \frac{z_i u_i F}{D_4} \frac{\partial}{\partial \xi}\left(c_i \frac{\partial \Phi}{\partial \xi}\right) + 3t^{3/2}\xi^2 \frac{\partial c_i}{\partial \xi} + \frac{D_i}{D_4} \frac{\partial^2 c_i}{\partial \xi^2} \right\}, \tag{17}$$

$$t\left(\frac{\partial c_4}{\partial t}\right)_\xi = \frac{\xi}{2} \frac{\partial c_4}{\partial \xi} + \frac{z_4 u_4 F}{D_4} \frac{\partial}{\partial \xi}\left(c_4 \frac{\partial \Phi}{\partial \xi}\right) + 3t^{3/2}\xi^2 \frac{\partial c_4}{\partial \xi} + \frac{\partial^2 c_4}{\partial \xi^2}, \tag{18}$$

and

$$-F^2 \frac{\partial}{\partial \xi}\left(\frac{\partial \Phi}{\partial \xi} \sum_{i=1}^{4} z_i^2 u_i c_i\right) - F \sum_{i=1}^{4} z_i D_i \frac{\partial^2 c_i}{\partial \xi^2} = 0 . \tag{19}$$

Equations (17) to (19) are the forms of the material balance and the charge conservation relationships that are solved numerically in the electrolytic solution. The equilibrium and electroneutrality equations are applied directly.

Boundary conditions in the bulk solution

In the bulk solution, it is assumed that the ferrous ion concentration is zero. The HSO_4^-, H^+, and SO_4^{--} concentrations are determined by the specified bulk concentration of sulfuric acid, the equilibrium expression, and the electroneutrality equation. If $c^\infty_{H_2SO_4}$ is the bulk concentration of sulfuric acid, then

$$c_1(\xi_{max}) = \frac{(3c^\infty_{H_2SO_4} + K) - \left((3c^\infty_{H_2SO_4} + K)^2 - 8\,(c^\infty_{H_2SO_4})^2\right)^{1/2}}{2}, \tag{20}$$

where K is the equilibrium constant in Equation (6). The other bulk concentrations become:

$$c_2(\xi_{max}) = 2c^\infty_{H_2SO_4} - c_1(\xi_{max}) , \tag{21}$$

$$c_3(\xi_{max}) = c^{\infty}_{H_2SO_4} - c_1(\xi_{max}) , \tag{22}$$

and

$$c_4(\xi_{max}) = 0 . \tag{23}$$

The potential may be set equal to zero at ξ_{max} because only gradients of potential enter in the material balance equations.

$$\Phi(\xi_{max}) = 0 . \tag{24}$$

Boundary conditions at the electrode surface

The reduced flux of species i at the electrode-salt film interface, N_i^{sur}, is given by

$$N_i^{sur} = -z_i u_i F c_i \left.\frac{\partial \Phi}{\partial \xi}\right|_{\xi=0} - D_i \left.\frac{\partial c_i}{\partial \xi}\right|_{\xi=0} . \tag{25}$$

The flux of total hydrogen and total sulfate must be zero at the electrode surface. This leads to the following conditions:

$$N_1^{sur} = -N_2^{sur} , \tag{26}$$

and

$$N_1^{sur} = -N_3^{sur} . \tag{27}$$

Equilibrium, Equation (6), and electroneutrality, Equation (4), are applied at the electrode surface.

The final boundary condition is a kinetic expression that determines the flux of ferrous ions due to dissolution of the electrode. A Butler-Volmer relationship having the same form as used by Law and Newman[13] is presumed to apply:

$$i_{bv} = nFk_a \exp\left[\frac{\alpha_a F}{RT}\left(V - \Phi_o\right)\right] - nFk_c c_4 \exp\left[-\frac{\alpha_c F}{RT}\left(V - \Phi_o\right)\right]. \tag{28}$$

The reference electrode of a given kind is a normal hydrogen electrode. Kinetic data obtained from a rotating hemispherical electrode in a 1 M sulfuric acid electrolyte are illustrated in Figure 2. The data have been corrected for ohmic drop. Values of k_a and k_c were chosen so that Equation

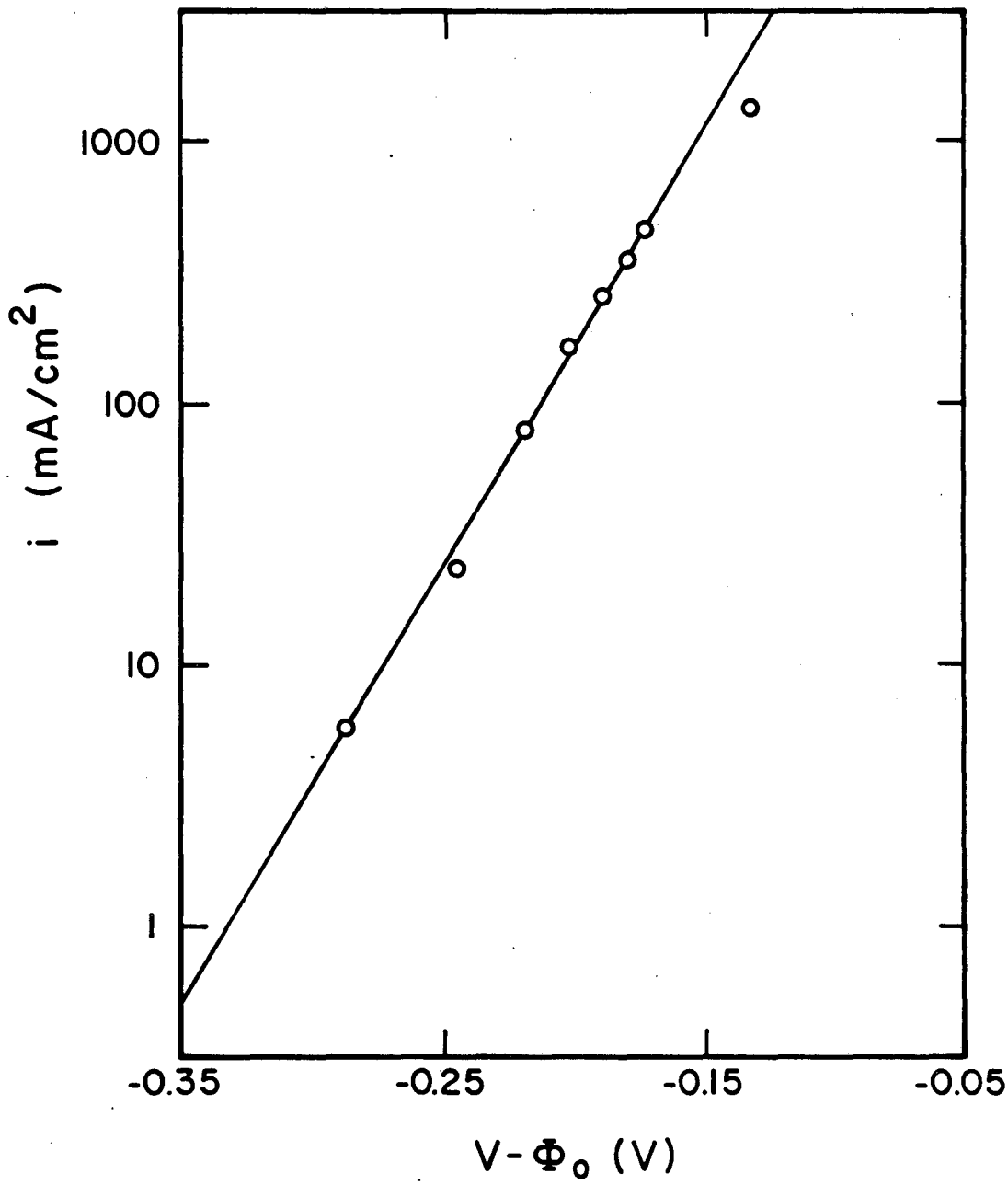

Figure 2. Kinetic data obtained from a rotating hemispherical electrode in 1 M H_2SO_4. Temperature was 25±0.1°C.

(28) agrees closely with the data. The curve determined by Equation (28) is included in Figure 2 for comparison with the data.

The Tafel slope for the data is 60 mV/decade. Bockris, Drazic, and Despic[14] reported Tafel slopes of 60 mV/decade when they did not subject the electrolyte to special purification steps. These results are in agreement with their work for low pH electrolytes composed of reagent grade chemicals.

The flux of ferrous ions is expressed in terms of the current density.

$$\left\{-z_4 u_4 F c_4 \frac{\partial \Phi}{\partial \xi}\bigg|_{\xi=0} - D_4 \frac{\partial c_4}{\partial \xi}\bigg|_{\xi=0}\right\}\left(\frac{a\nu}{3D_4}\right)^{1/3}\left(\frac{\Omega}{\nu}\right)^{1/2}\frac{1}{\sqrt{t}} = \frac{i}{nF}. \tag{29}$$

The electrode surface is assumed to be uncovered during phase 1, so that the superficial current density, i, may be equated with the Butler-Volmer current density calculated in Equation (28).

It should be emphasized that the hemispherical electrode was used to provide kinetic data because of the uniform potential distribution associated with this geometry. This model, however, is a simulation of salt-film formation on a disk electrode.

Calculation of $V - \Phi_o$

The experiments yield values of the electrode potential relative to a reference electrode of a given kind. The reference electrode is located in the bulk solution, essentially at infinity. The numerical simulation calculates the potential difference between a point just outside the diffuse double layer and a point just beyond the diffusion layer. The ohmic potential drop in the bulk electrolyte must now be included in the calculation. Figure 3 is a one-dimensional plot indicating the various potentials relevant to the problem. The potential difference $V - \Phi_{RE}$ is separated in the following manner

$$V - \Phi_{RE} = (V - \Phi_o) + (\Phi_o - \Phi_{\xi_{max}}) + (\tilde{\Phi}_o - \Phi_{RE}) - (\tilde{\Phi}_o - \Phi_{\xi_{max}}). \tag{30}$$

The second term on the right side of Equation (30) is the potential difference

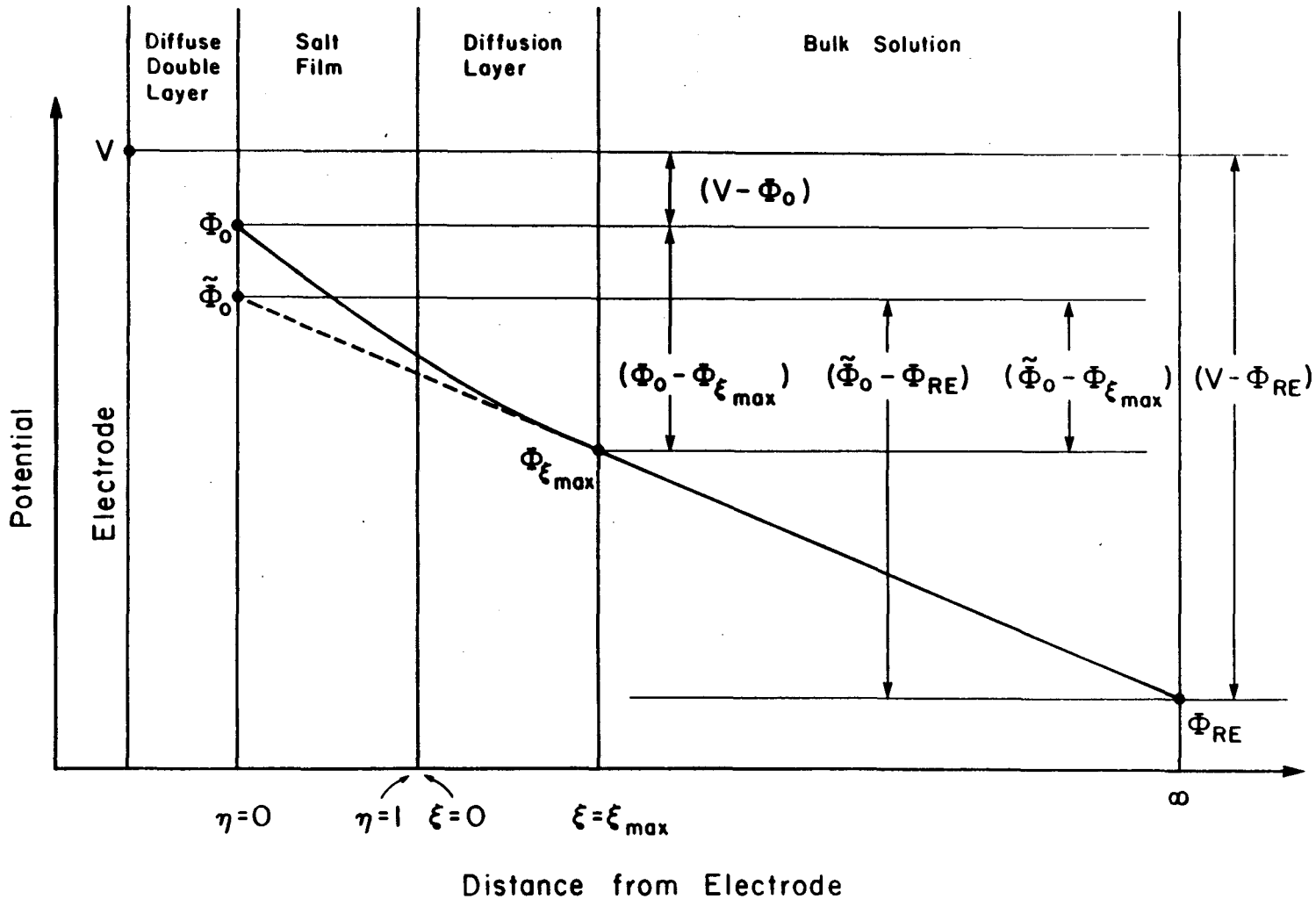

Figure 3. Breakdown of $(V - \Phi_{RE})$ into a number of tractable components.

determined by the numerical simulation as described above. This term contains an ohmic component that accounts for variations in electrolyte conductivity and a diffusion potential. Note that $\Phi_{\xi_{max}} = 0$ according to Equation (24).

The third term on the right side is the ohmic potential drop between the plane just outside the diffuse double layer and a hemispherical counterelectrode located at infinity, assuming the conductivity is constant and equal to the bulk solution value. The one-dimensional character of the model requires i to be independent of radial position. The total current is

$$I = \pi r_o^2 i \ . \tag{31}$$

The ohmic resistance is estimated to be equal to the resistance for a primary current distribution on the surface of the disk, $1/4\kappa_{H_2SO_4} r_o$.[15] The ohmic potential difference is then

$$\tilde{\Phi}_o - \Phi_{RE} = i \frac{\pi r_o}{4\kappa_{H_2SO_4}} . \tag{32}$$

The ohmic potential drop in the diffusion layer is implicitly contained in both the second and the third terms on the right side of Equation (30). This can be seen in Figure 3. To avoid counting this contribution twice, it must be subtracted; this is the purpose of the fourth term on the right side of Equation (30). The fourth term may be rewritten as

$$\tilde{\Phi}_o - \Phi_{\xi_{max}} = \frac{i\sqrt{t}\,\xi_{max}}{\left(\frac{a\,\nu}{3\,D_4}\right)^{1/3}\left(\frac{\Omega}{\nu}\right)^{1/2}\kappa_{H_2SO_4}} . \tag{33}$$

Substitution of Equations (32) and (33) into (30), and rearrangement gives

$$(V - \Phi_o) = (V - \Phi_{RE}) - (\Phi_o - \Phi_{\xi_{max}}) - \frac{i}{\kappa_{H_2SO_4}}\left(\frac{\pi r_o}{4} - \frac{\sqrt{t}\,\xi_{max}}{\left(\frac{a\,\nu}{3\,D_4}\right)^{1/3}\left(\frac{\Omega}{\nu}\right)^{1/2}}\right) . \tag{34}$$

Substitution of Equation (34) into (28) results in a kinetic equation that

contains the current density as an unknown.

$$\frac{i}{nF} = k_a \exp\left[\Psi_a\right] - k_c c_4 \exp\left[-\Psi_c\right], \tag{35}$$

where

$$\Psi_a = \frac{\alpha_a F}{RT}\left(V - \Phi_{RE}) - (\Phi_o - \Phi_{\xi_{max}}) - \frac{i}{\kappa_{H_2SO_4}}\left[\frac{\pi r_o}{4} - \frac{\sqrt{t}\,\xi_{max}}{\left(\frac{a\nu}{3D_4}\right)^{1/3}\left(\frac{\Omega}{\nu}\right)^{1/2}}\right]\right),$$

and

$$\Psi_c = \frac{\alpha_c F}{RT}\left(V - \Phi_{RE}) - (\Phi_o - \Phi_{\xi_{max}}) - \frac{i}{\kappa_{H_2SO_4}}\left[\frac{\pi r_o}{4} - \frac{\sqrt{t}\,\xi_{max}}{\left(\frac{a\nu}{3D_4}\right)^{1/3}\left(\frac{\Omega}{\nu}\right)^{1/2}}\right]\right).$$

Current density is not explicitly treated as a variable in the numerical simulation. Equation (29) replaces the current density in this kinetic equation with variables and parameters that are explicitly carried in the numerical simulation.

Newman's method[16] is used to solve for the concentration and potential profiles as functions of position. Time steps are carried out with an implicit method where the old and the new values are equally weighted. This is known as the Crank-Nicholson procedure.[17]

Modification of the Butler-Volmer equation

Convergence was very slow when Equation (35) was programmed directly. More than 12 iterations were required to obtain convergence to 10 significant figures. Rapid convergence may be obtained if the logarithm of Equation (35) is used

$$\ln\left[\frac{nF}{i}\left(k_a e^{\Psi_a} - k_c c_4 e^{-\Psi_c}\right)\right] = 0\,. \tag{36}$$

Again, Equation (29) is substituted for the current density when it appears in

Equation (36).

The superior convergence of the logarithmic form is illustrated in Figure 4. The error in the equation is plotted after each iteration. Four iterations were sufficient to achieve a relative convergence of 10 significant figures for the logarithmic form. More than 12 iterations were required for the same level of convergence with the algebraic form, Equation (35). The algebraic form reduces the error by a factor of e^{-1} on each of the first 8 iterations. This is the expected behavior for a Newton-Raphson iteration scheme applied to an exponential function for an initial guess that is far from the answer. By working with the logarithm of the equation, the curvature of the exponential is tremendously reduced, and convergence is achieved much more rapidly.

Physical property data

The program requires a number of physical property values and other data. These are summarized in Table 1.

The product of viscosity and diffusivity is approximately constant. The relative viscosities of $CdSO_4$ solutions range between 3.0 and 5.1 for concentrations between 1.75 and 2.50 *M* at a temperature of 25°C.[18] High concentrations are expected because Beck[3] has observed a minimum supersaturation concentration of 1.8 times the saturated value before the onset of precipitation. Solutions of copper sulfate, magnesium sulfate, and zinc sulfate have relative viscosity dependencies on concentration that are similar to that for $CdSO_4$.[19] It seems reasonable to assume that the relative viscosity dependence on concentration for $FeSO_4$ will be similar to that for $CdSO_4$. Therefore, the values of the mobilities and the diffusivities listed in Table 1 have been reduced by a factor of four from their values at infinite dilution.[6]

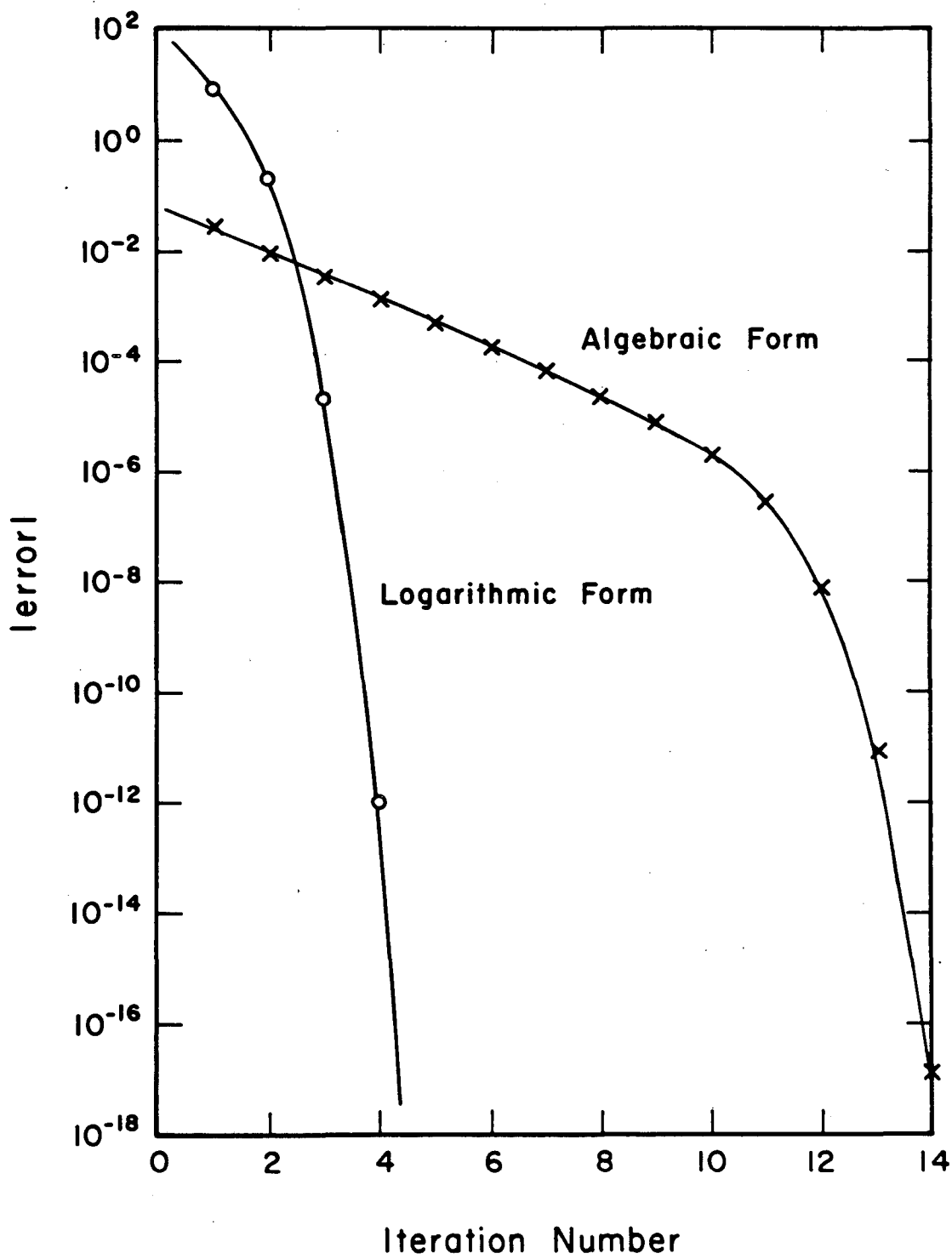

Figure 4 Speed of convergence is compared for the algebraic form and the logarithmic form of the Butler-Volmer equation.

Table 1.

Input data for mathematical model.

A. Transport properties

Species	$u_i \times 10^9$ $\frac{cm^2\text{-mol}}{J\text{-}s}$	$D_i \times 10^5$ $\frac{cm^2}{s}$	z_i	s_i
HSO_4^-	1.343	0.3323	-1	0
H^+	9.394	2.328	1	0
SO_4^{--}	1.074	0.2663	-2	0
Fe^{++}	0.6688	0.1658	2	-1

B. Other input parameters

Symbol	Value	Description	Dimension
a	0.51023	Disk hydrodynamic constant	
$c^{sat}_{FeSO_4}$	1.88	Saturation concentration[20]	M
k_a	2.0052×10^{-3}	Anodic rate constant	$mol/cm^2\text{-}s$
k_c	2.6701×10^{-15}	Cathodic rate constant	cm/s
n	2	Equivalents per mol Fe^{++}	
r_o	0.1491	Electrode radius	cm
R	8.3143	Gas constant	J/mol-K
T	298.15	Absolute temperature	K
α_a	1.0	Anodic transfer coefficient	
α_c	1.0	Cathodic transfer coefficient	
$\kappa_{H_2SO_4}$	0.40	Conductivity	$\Omega^{-1}\text{-}cm^{-1}$
ν	0.0398	Kinematic viscosity	cm^2/s
ξ_{max}	6.0	Max. dimensionless distance	

Results for phase 1

Table 2 lists the surface concentration of each ionic species, the value of the current density, and the dimensionless time at the completion of selected time steps during the concentration buildup process. The value of the bisulfate-sulfate equilibrium constant was set equal to 5×10^{-5} mol/cm^3.

The concentration buildup ends when the ferrous ion concentration exceeds a value 1.8 times greater than the saturated concentration of ferrous sulfate. A calculated time of 1.75 s is required to exceed this maximum supersaturation concentration. The concentration profiles at this instant in

Table 2.

Values of the surface concentrations and the current density as functions of the dimensionless time during phase 1.

	Surface Concentrations (M)				
t	c_1	c_2	c_3	c_4	i (A/cm^2)
5.623×10^{-5}	0.9763	1.004	0.04862	0.03482	2.372
1.000×10^{-4}	0.9919	0.9753	0.05085	0.05916	2.369
1.778×10^{-4}	1.008	0.9462	0.05327	0.08422	2.366
3.162×10^{-4}	1.029	0.9102	0.05651	0.1158	2.362
5.623×10^{-4}	1.054	0.8669	0.06081	0.1545	2.357
1.778×10^{-3}	1.129	0.7503	0.07525	0.2647	2.341
5.623×10^{-3}	1.248	0.5891	0.1059	0.4355	2.314
1.778×10^{-2}	1.424	0.3943	0.1805	0.6952	2.269
5.623×10^{-2}	1.627	0.2112	0.3852	1.093	2.194
1.778×10^{-1}	1.760	0.09957	0.8836	1.714	2.085
5.623×10^{-1}	1.881	0.05806	1.620	2.531	1.986
8.700×10^{-1}	2.005	0.05526	1.814	2.789	1.952
1.562×10^{0}	2.128	0.05269	2.020	3.058	1.932
3.120×10^{0}	2.032	0.04132	2.459	3.454	1.915

time are plotted in Figure 5. Only the region on the abscissa between $x = 0$ and $x = 5$ should be considered. The potential labeled $\Phi(t_{0-})$ is the relevant potential profile. At this time, the position at $x = 0$ represents the electrode surface. The regions on the abscissa corresponding to the variables η and ξ are results from the initial salt-film-formation problem, which will be considered in the next section.

Ateya and Pickering[21] present a stagnant-diffusion-layer model that predicts the formation of salt films. Their concentration profiles are qualitatively similar to the ones presented in Figure 5 for values of x between 0 and 5.

Initial salt-film formation

We now consider what physical steps occur at the initial instant of salt-film formation. The surface concentration of ferrous ions is assumed to fall to the saturation concentration of $FeSO_4$ from the maximum supersaturation value. This process is illustrated in Figure 5. The relevant region is for abscissa values between $\xi = 0$ and $\xi = 6$. The steep positive concentration gradient is responsible for a flux of ferrous ions that will form the salt film. The dimensionless time, t, is assumed to be reset equal to zero at this instant. As time proceeds, the following steps occur:

(*i*) Diffusion of ferrous ions from the bulk solution causes the salt film to thicken. Initially, the film thickness is approximately proportional to the square root of time.

(*ii*) The maximum ferrous ion concentration transiently decreases. This is due to dissipation down the positive concentration gradient, feeding salt-film growth, and to dissipation down the negative concentration gradient toward the bulk solution, where the concentration is zero.

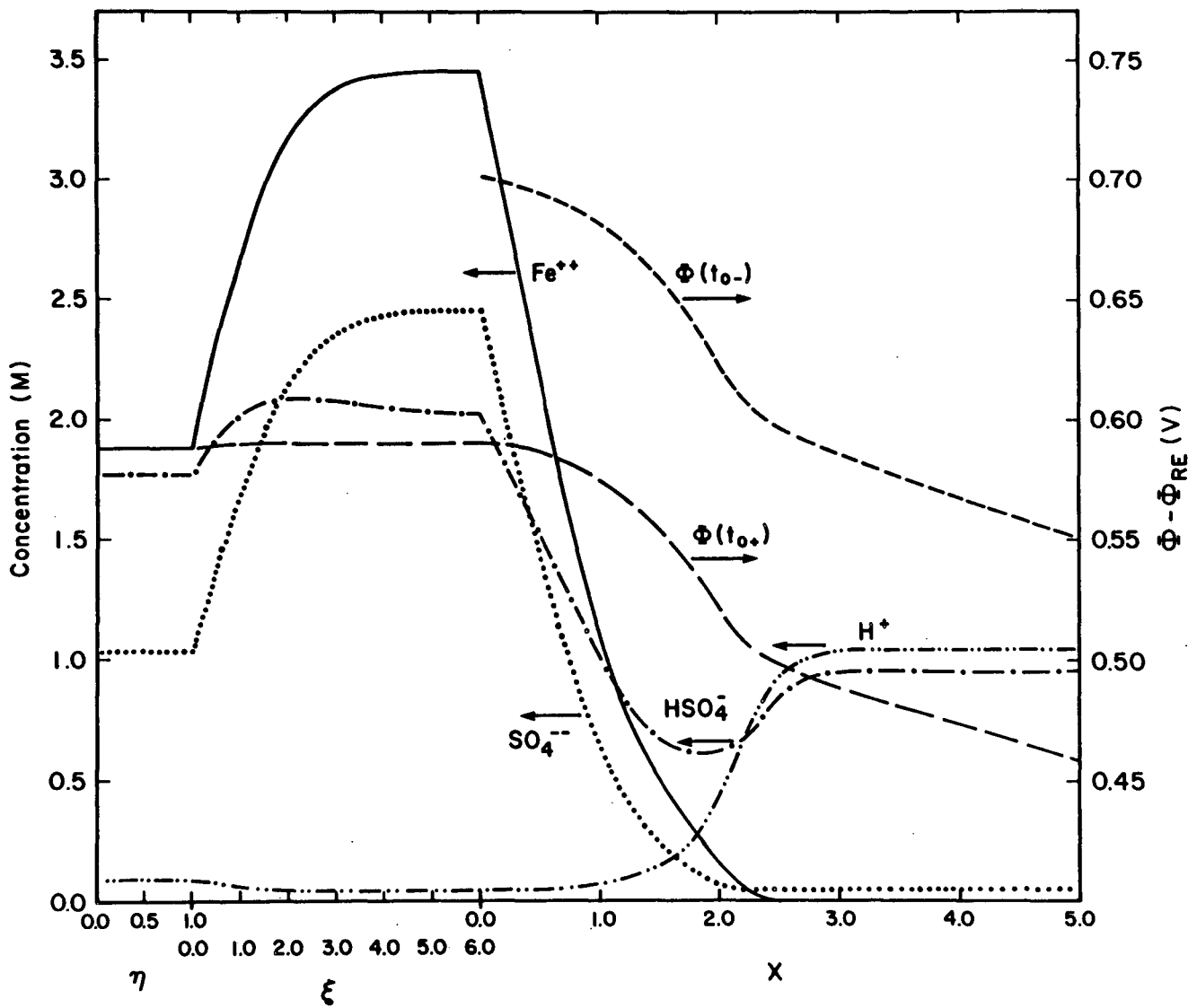

Figure 5. Potential and concentration profiles at t_{o-} are shown for values on the abscissa of $0 < x < 5$. At t_{o-}, the electrode surface is located at $x = 0$. Potential and concentration profiles at t_{o+} in the salt film (abscissa variable η) and solution region described by the stretched variable ξ are included. The profiles on x are unchanged at t_{o+}.

(*iii*) Continued corrosion at the electrode surface increases the ferrous concentration in the pores of the salt film. This source of ferrous ions permits the continued existence of the salt film on the limiting current plateau. At limiting current, the ferrous concentration is a monotonically decreasing function with distance away from the electrode surface. The flux of ferrous ions dissolving at the electrode surface exactly matches the dissolution rate of the salt film. This concept will be treated in more detail in part II of this series.

Mathematical model for initial salt-film formation

The equations used to describe the initial salt-film formation process are now derived. The concentration profiles on Figure 5 between $x = 0$ and $x = 5$ are stored in the computer memory. These profiles are used to determine boundary conditions for the problem defined below.

Equations (6), (4), and (12) to (14) are the starting point for this model. The distance domain is separated into two distinct regions: the porous salt film and the electrolyte solution near the salt film-solution interface. The salt-film thickness, δ_y, is included as an additional unknown in this problem. The salt-film thickness is a function of time; however, it is independent of distance. The following is used as the governing equation for the salt-film thickness.

$$\frac{d\delta_y}{dy} = 0 . \tag{37}$$

The coordinate transformations used in these two regions are now presented.

Co-ordinate transformation for the solution region

A distance variable for the electrolytic solution region is chosen so that it always has a value of zero at the salt film-solution interface; it is stretched in the time variable to facilitate monitoring the transient concentration

profiles accompanying growth of the salt film.

$$\xi = \frac{x - \delta_x}{\sqrt{t}}, \tag{38}$$

where δ_x is a dimensionless salt-film thickness obtained by multiplying δ_y by the factor in Equation (11). It should be emphasized that t is reset to zero at the instant of initial precipitation.

The transformation of the time derivatives evaluated at constant x to time derivatives at constant ξ is analogous to Equation (16).

$$\left(\frac{\partial c_i}{\partial t}\right)_x = \left(\frac{\partial c_i}{\partial t}\right)_\xi + \left(-\frac{\xi + \delta_x/\sqrt{t}}{2t} - \frac{d(\delta_x/\sqrt{t})}{dt}\right)\left(\frac{\partial c_i}{\partial \xi}\right)_t . \tag{39}$$

For notational convenience, let

$$\delta = \frac{\delta_x}{\sqrt{t}} . \tag{40}$$

Substitution of this transformation into Equations (12) to (14) gives

$$\sum_{i=1}^{2}\left\{t\left(\frac{\partial c_i}{\partial t}\right)_\xi - t\frac{d\delta}{dt}\frac{\partial c_i}{\partial \xi}\right\} = \sum_{i=1}^{2}\left\{\frac{1}{2}(\xi+\delta)\frac{\partial c_i}{\partial \xi} + \frac{z_i u_i F}{D_4}\frac{\partial}{\partial \xi}\left(c_i\frac{\partial \Phi}{\partial \xi}\right)\right.$$

$$\left. + 3t^{3/2}\xi^2\frac{\partial c_i}{\partial \xi} + \frac{D_i}{D_4}\frac{\partial^2 c_i}{\partial \xi^2}\right\}, \tag{41}$$

$$t\left(\frac{\partial c_4}{\partial t}\right)_\xi - t\frac{d\delta}{dt}\frac{\partial c_4}{\partial \xi} = \frac{1}{2}(\xi+\delta)\frac{\partial c_4}{\partial \xi} + \frac{z_4 u_4 F}{D_4}\frac{\partial}{\partial \xi}\left(c_4\frac{\partial \Phi}{\partial \xi}\right)$$

$$+ 3t^{3/2}\xi^2\frac{\partial c_4}{\partial \xi} + \frac{\partial^2 c_4}{\partial \xi^2}, \tag{42}$$

and

$$-F^2\frac{\partial}{\partial \xi}\left(\frac{\partial \Phi}{\partial \xi}\sum_{i=1}^{4} z_i^2 u_i c_i\right) - F\sum_{i=1}^{4} z_i D_i\frac{\partial^2 c_i}{\partial \xi^2} = 0 . \tag{43}$$

Equations (41) and (42) are the material balance relationships for the

electrolytic solution. Equation (43) is the charge conservation relationship for the electrolytic solution. The equilibrium and electroneutrality equations are applied directly. The governing equation for the salt-film thickness becomes

$$\frac{d\delta}{d\xi} = 0 . \tag{44}$$

Co-ordinate transformation for the porous salt film

A reduced distance variable, η, within the salt film is defined by

$$\eta = \frac{x}{\delta_x} . \tag{45}$$

The electrode-salt film boundary is located at $\eta = 0$. The salt film-electrolyte boundary is located at $\eta = 1$.

The transformation to convert from time derivatives at constant x to time derivatives at constant η is

$$\begin{aligned}\left(\frac{\partial c_i}{\partial t}\right)_x &= \left(\frac{\partial c_i}{\partial t}\right)_\eta \left(\frac{\partial t}{\partial t}\right)_x + \left(\frac{\partial c_i}{\partial \eta}\right)_t \left(\frac{\partial (x/\delta_x)}{\partial t}\right)_x \\ &= \left(\frac{\partial c_i}{\partial t}\right)_\eta - \frac{\eta}{2}\frac{1}{\delta_x^2}\frac{d\delta_x^2}{dt}\frac{\partial c_i}{\partial \eta} \\ &= \left(\frac{\partial c_i}{\partial t}\right)_\eta - \frac{\eta}{2}\frac{1}{t\delta^2}\frac{d(t\delta^2)}{dt}\frac{\partial c_i}{\partial \eta} .\end{aligned} \tag{46}$$

Substitution of this transformation into Equations (12) to (14) gives:

$$\sum_{i=1}^{2}\left\{t\delta^2\left(\frac{\partial c_i}{\partial t}\right)_\eta - \frac{\eta}{2}\frac{d(t\delta^2)}{dt}\frac{\partial c_i}{\partial \eta}\right\} = \sum_{i=1}^{2}\left\{\frac{z_i u_i F}{D_4}\frac{\partial}{\partial \eta}\left(c_i\frac{\partial \Phi}{\partial \eta}\right) + \frac{D_i}{D_4}\frac{\partial^2 c_i}{\partial \eta^2}\right\}, \tag{47}$$

$$t\delta^2\left(\frac{\partial c_4}{\partial t}\right)_\eta - \frac{\eta}{2}\frac{d(t\delta^2)}{dt}\frac{\partial c_4}{\partial \eta} = \frac{z_4 u_4 F}{D_4}\frac{\partial}{\partial \eta}\left(c_4\frac{\partial \Phi}{\partial \eta}\right) + \frac{\partial^2 c_4}{\partial \eta^2} , \tag{48}$$

and

$$-F^2 \frac{\partial}{\partial \eta}\left(\frac{\partial \Phi}{\partial \eta} \sum_{i=1}^{4} z_i^2 u_i c_i\right) - F \sum_{i=1}^{4} z_i D_i \frac{\partial^2 c_i}{\partial \eta^2} = 0 . \tag{49}$$

These are the material balances and the charge conservation relationship for the pores of the salt film. The porosity in the salt film, ϵ_f, is assumed to be a constant, independent of position in the film. The porosity is accounted for in the formulation of the boundary conditions; it does not explicitly appear in Equations (47) to (49). The velocity is assumed to equal zero in the pores of the salt film, so no convection term is included in the above equations. The equilibrium and electroneutrality equations are applied directly. The governing equation for the salt-film thickness becomes

$$\frac{d\delta}{d\eta} = 0 . \tag{50}$$

Structure of equations

Figure 6 maps the layout of equations. The left side represents the electrode surface. The salt film-solution interface is located at the center of the horizontal lines. The column labeled $\xi = \xi_{max}$ is a position in the electrolyte at the value of x corresponding to ξ_{max}.

Each governing equation is represented by a horizontal line. The corresponding unknown is listed in the right column. Positions where boundary conditions are required are indicated by an open square.

The first horizontal line represents Equation (47) in the salt-film region and Equation (41) in the solution region.

The second line represents Equation (49) in the salt-film region and Equation (43) in the solution region. Two boundary conditions are required for this equation because it is a second-order differential equation, as can be seen by inspection of Equation (49) or (43). A matching condition is also required at the salt film-solution interface to allow for the change in porosity at this location.

Structure of Equations

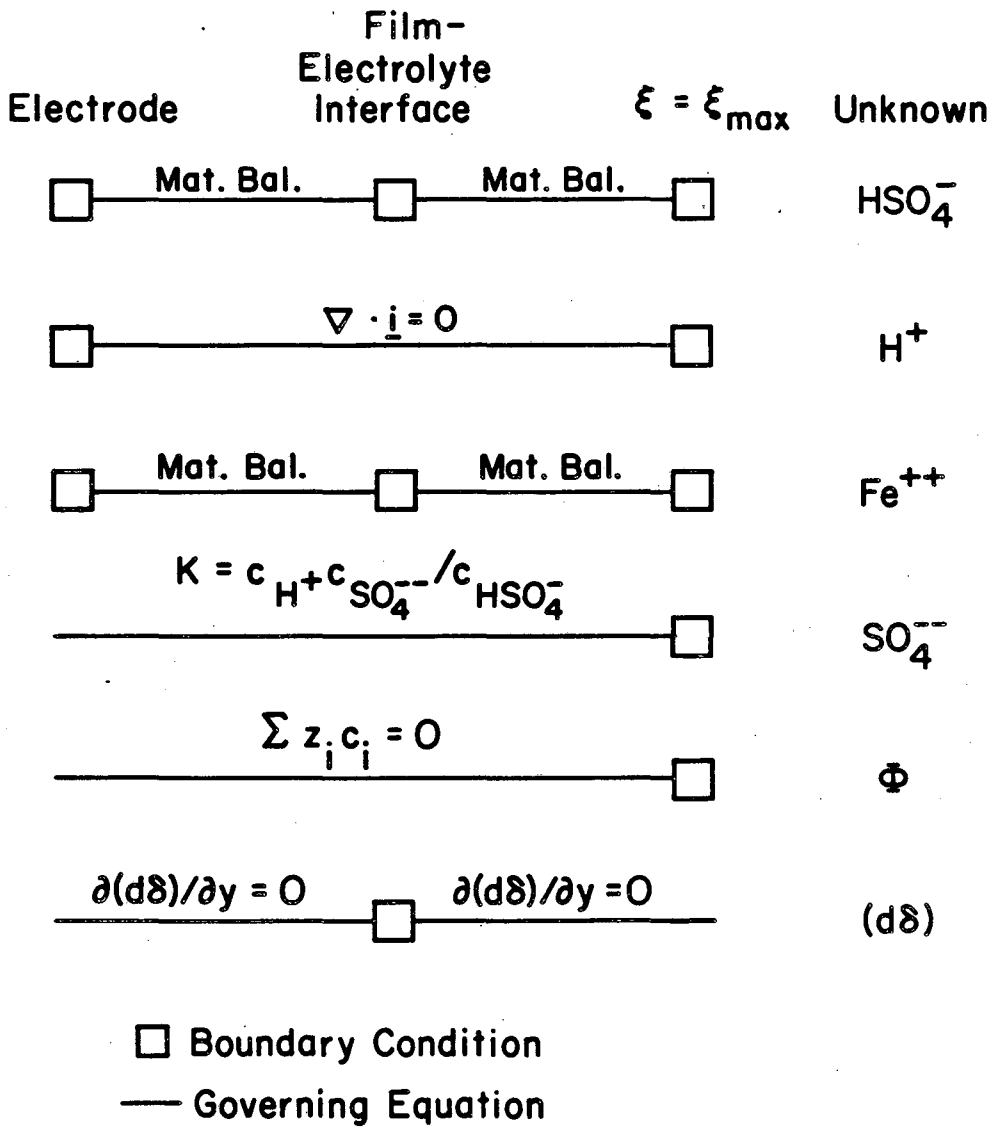

Figure 6. Structure of the equations for the salt film-solution geometry. Boundary conditions are indicated by an open square.

The third line represents Equation (48) in the salt-film region and Equation (42) in the solution region.

The fourth and fifth lines represent Equations (6) and (4), respectively, in both the salt-film and the solution regions.

The sixth line represents Equation (50) in the salt film and Equation (44) in the solution. The variable $d\delta$ is the change in δ that occurs during a time-step dt. The quantity $d\delta$ should not be thought of as a differential, but as a difference variable indicating the change in salt film thickness occurring in a finite time.

Boundary conditions at ξ_{max}

The boundary conditions at ξ_{max} are established by calculating the corresponding position in terms of the variable x.

$$x_{\xi_{max}} = \sqrt{t}\,(\xi_{max} + \delta)\,. \tag{51}$$

The concentration profiles on Figure 5 between $x = 0$ and $x = 5$ are termed the "long" profiles. The values on the long concentration profiles at $x = x_{\xi_{max}}$ are the values selected for the boundary conditions. In equation form,

$$c_i(\xi_{max}) = c_{long,i}(x = x_{\xi_{max}})\,; \quad i = 1 \text{ to } 4\,. \tag{52}$$

For example, at zero time, $x_{\xi_{max}} = 0$; the boundary condition at ξ_{max} for the ferrous ion is the maximum supersaturation concentration. As time moves on, the ionic concentrations selected for these boundary conditions are values that exist on the long profiles further away from the film-solution interface.

The first four boxes in the column labeled $\xi = \xi_{max}$ on Figure 6 correspond to Equation (52) with i = 1-4. The fifth box is the boundary condition for the potential which is taken as

$$\Phi_{\xi_{max}} = 0\,. \tag{53}$$

Equation (44) for the film thickness is applied directly at this location.

Boundary conditions at film-solution interface

The net flux of any species at the film-solution interface is defined as the flux arriving from the pores of the salt film less the flux moving into the electrolyte.

$$N_i^{net} = N_i^f - N_i^s \,, \tag{54}$$

where

$$N_i^f = \epsilon_f \left\{ -z_i u_i F c_i \left. \frac{\partial \Phi}{\partial \eta} \right|_{\eta = 1} - D_i \left. \frac{\partial c_i}{\partial \eta} \right|_{\eta = 1} \right\}, \tag{55}$$

and

$$N_i^s = \delta \left\{ -z_i u_i F c_i \left. \frac{\partial \Phi}{\partial \xi} \right|_{\xi = 0} - D_i \left. \frac{\partial c_i}{\partial \xi} \right|_{\xi = 0} \right\}. \tag{56}$$

The bracketed terms on the right side of Equation (55) represent a reduced flux in the pores of the salt film. This quantity is multiplied by the film porosity, ϵ_f, so that a superficial flux results.

The interfacial boundary conditions are now listed in terms of the net flux expressions.

The net flux of ferrous ions must equal the net flux of total sulfate. This is because formation or dissolution of ferrous sulfate consumes or releases an equal number of ferrous and sulfate ions.

$$N_4^{net} = N_1^{net} + N_3^{net} \,. \tag{57}$$

The first box in the Film-Electrolyte Interface column on Figure 6 represents Equation (57).

The charge conservation equation is applied directly at the salt film-solution interface. The current density flowing out of the salt-film pores is equated to the current density flowing into the electrolyte. Care must be taken to account for the porosity of the salt film correctly.

The ferrous concentration is fixed at the saturation concentration of ferrous sulfate at the interface.

$$c_4(\xi = 0) = c^{sat}_{FeSO_4} \,. \tag{58}$$

The second box in the Film-Electrolyte Interface column on Figure 6 represents Equation (58).

Equilibrium, Equation (6), and electroneutrality, Equation (4), are applied directly.

The final relationship is a material balance on the ferrous species that determines the change in the thickness of the salt film.

$$(1 - \epsilon_f)\, D_4\, \rho_f\, (\sqrt{t}\,\delta) \frac{d(\sqrt{t}\,\delta)}{dt} = N_4^{net} \,. \tag{59}$$

This equation is similar to one derived by Tiedemann and Newman.[22] The last box in the Film-Electrolyte Interface column of Figure 6 represents Equation (59).

Boundary conditions at the electrode surface

The reduced flux of species i at the electrode-salt film interface, N_i^{sur}, is given by

$$N_i^{sur} = -z_i u_i F c_i \left.\frac{\partial \Phi}{\partial \eta}\right|_{\eta = 0} - D_i \left.\frac{\partial c_i}{\partial \eta}\right|_{\eta = 0} \,. \tag{60}$$

The flux of total hydrogen and total sulfate must be zero at the electrode surface. This leads to the following conditions:

$$N_1^{sur} = -N_2^{sur} \,, \tag{61}$$

and

$$N_1^{sur} = -N_3^{sur} \,. \tag{62}$$

The first two boxes in the Electrode column of Figure 6 represent Equations (61) and (62).

Equilibrium, Equation (6), and electroneutrality, Equation (4), are applied at the electrode surface. Equation (50) for the salt-film thickness is also applied at the electrode surface.

The third box in the Electrode column of Figure 6 represents the Butler-Volmer kinetic expression given in Equation (28). Formation of the salt film may result in a certain fraction of the surface being blocked, and therefore unable to undergo dissolution. The fraction of the electrode area that is not blocked is denoted as ϵ_s, the surface porosity. The superficial current density, i, is related to the Butler-Volmer current density, i_{bv}, and to the pore current density by the following relationship:

$$i = \epsilon_s \, i_{bv} = \epsilon_f \, i_p \, . \tag{63}$$

The salt-film porosity, ϵ_f, is not necessarily equal to the surface porosity.

The flux of ferrous ions at the electrode-film interface is related to the superficial current density by

$$\left\{ -z_4 u_4 F c_4 \frac{\partial \Phi}{\partial \eta}\bigg|_{\eta=0} - D_4 \frac{\partial c_4}{\partial \eta}\bigg|_{\eta=0} \right\} \left(\frac{a\nu}{3D_4}\right)^{1/3} \left(\frac{\Omega}{\nu}\right)^{1/2} \frac{1}{\sqrt{t\,\delta}} = \frac{i}{\epsilon_f n F} \, . \tag{64}$$

Calculation of V - Φ_o

Let t_{o-} represent the instant just before the first crystal of $FeSO_4$ precipitates; t_{o+} is the instant just after initial precipitation. At t_{o-}, the potential difference $\Phi_o - \Phi_{x_{max}}$ is the sum of the ohmic drop and the diffusion potential that exists between $x = 0$ and $x = 5$ as defined on Figure 5.* In equation form,

*Concentration profiles are calculated to $x_{max} = 6$ in the computer program. Figure 5 only extends to $x = 5$ because the concentrations are essentially uniform for larger values of x. The variable ξ is defined in the context of Equation (15) when $t \leq t_{o-}$. The time variable is reset to zero only after the initial salt crystal formation at $t = t_{o+}$.

$$(\Phi_o - \Phi_{\xi_{max}})\Big|_{t_o-} = (\Phi_o - \Phi_{x_{max}})\Big|_{t_o-}$$

$$= i(t_o-)\int_0^{x_{max}} \frac{dx}{\kappa} + F\int_0^{x_{max}} \frac{\sum_{i=1}^{4} z_i D_i \frac{\partial c_i}{\partial x}}{\kappa} dx \ . \tag{65}$$

For values of $t > t_{o+}$, the quantity $(\Phi_o - \Phi_{\xi_{max}})\Big|_{t > t_{o+}}$ represents the sum of the ohmic drop and the diffusion potential from $x = 0$ to $x_{\xi_{max}}$, or

$$(\Phi_o - \Phi_{\xi_{max}})\Big|_{t > t_{o+}} = i(t>t_{o+})\int_0^{x_{\xi_{max}}} \frac{dx}{\kappa} + F\int_0^{x_{\xi_{max}}} \frac{\sum_{i=1}^{4} z_i D_i \frac{\partial c_i}{\partial x}}{\kappa} dx \ . \tag{66}$$

This quantity is initially much smaller than the quantity calculated in Equation (65) because $x_{\xi_{max}} < x_{max}$.** We want to include the ohmic drop and the diffusion potential associated with the outer part of the long profiles. The quantity we wish to calculate is the potential difference between the electrode surface and the position at x_{max}; this quantity is approximated by

$$(\Phi_o - \Phi_{x_{max}})\Big|_{t>t_{o+}} = i(t>t_{o+})\left[\int_0^{x_{\xi_{max}}} \frac{dx}{\kappa} + \int_{x_{\xi_{max}}}^{x_{max}} \frac{dx}{\kappa}\right]$$

$$+ F\left[\int_0^{x_{\xi_{max}}} \frac{\sum_{i=1}^{4} z_i D_i \frac{\partial c_i}{\partial x}}{\kappa} dx + \int_{x_{\xi_{max}}}^{x_{max}} \frac{\sum_{i=1}^{4} z_i D_i \frac{\partial c_i}{\partial x}}{\kappa} dx\right]. \tag{67}$$

This may be rewritten as

$$(\Phi_o - \Phi_{x_{max}})\Big|_{t>t_{o+}} = (\Phi_o - \Phi_{\xi_{max}})\Big|_{t>t_{o+}}$$

$$+ i(t>t_{o+})\int_{x_{\xi_{max}}}^{x_{max}} \frac{dx}{\kappa} + F\int_{x_{\xi_{max}}}^{x_{max}} \frac{\sum_{i=1}^{4} z_i D_i \frac{\partial c_i}{\partial x}}{\kappa} dx \ . \tag{68}$$

The first term on the right side of this equation is calculated according to the governing differential equations in the model. The last two terms on the right

**The variable ξ is defined in terms of Equation (38) for $t \geq t_{o+}$.

side are calculated from the long concentration profiles that are saved in the computer program. With Equation (68) the value of $(V - \Phi_o)$ in Equation (28) may be expressed as

$$(V - \Phi_o) = (V - \Phi_{RE}) - (\Phi_o - \Phi_{\xi_{max}}) - i \int_{x_{\xi_{max}}}^{x_{max}} \frac{dx}{\kappa} - F \int_{x_{\xi_{max}}}^{x_{max}} \frac{\sum_{i=1}^{4} z_i D_i \frac{\partial c_i}{\partial x}}{\kappa} dx$$
$$- (\tilde{\Phi}_o - \Phi_{RE}) + (\tilde{\Phi}_o - \Phi_{x_{max}}) . \tag{69}$$

This equation is analogous to Equation (34) and is obtained by reasoning that is similar to that illustrated in Figure 3. The fifth term on the right side of Equation (69) is given by Equation (32). The last term on the right side is given by

$$(\tilde{\Phi}_o - \Phi_{x_{max}}) = \frac{i x_{max}}{\left(\frac{a\nu}{3D_4}\right)^{1/3} \left(\frac{\Omega}{\nu}\right)^{1/2} \kappa_{H_2SO_4}} . \tag{70}$$

The boundary condition for the ferrous species at $\eta = 0$ is then represented by an equation analogous to Equation (35), where the superficial current density is replaced by Equation (64).

Solution technique

The domains in ξ and η are discretized as shown in Figure 7. The equations that were summarized in the discussion of Figure 6 are written in finite-difference form.

In the interior of either the salt-film region or the solution region, the material-balance equations are programmed in terms of fluxes that are evaluated between mesh points. This technique is described by Pollard[23] and utilized by Pollard and Newman.[24,25]

As before, Newman's method[16] is used to solve for the concentration and potential profiles as functions of position. Time steps are carried out with the

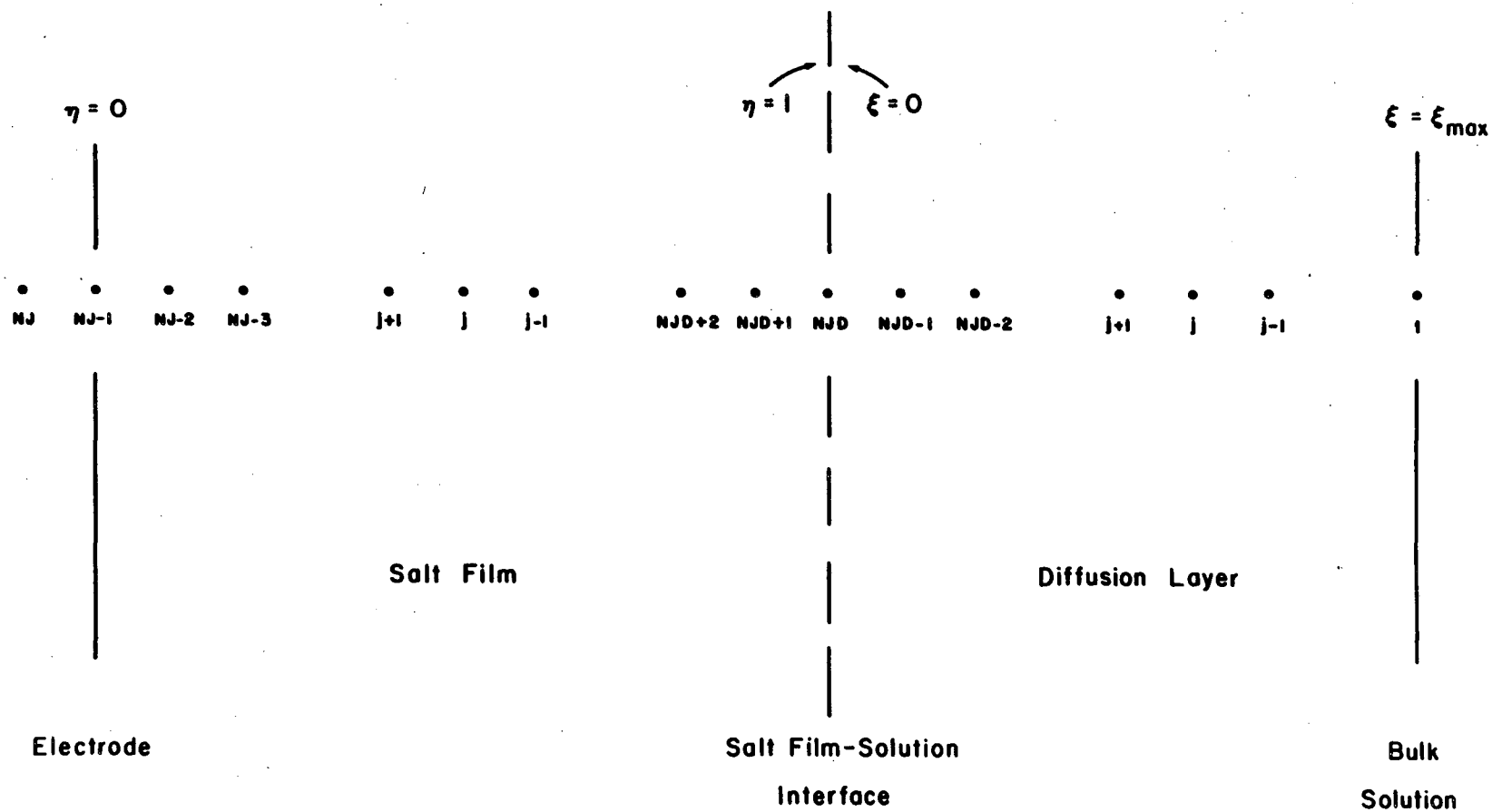

Figure 7. Discretization of η and ξ for numerical computations.

Crank-Nicholson procedure.[17] A more detailed description of the numerical solution technique can be found elsewhere.[26]

White[27] presents an alternative scheme for solving a problem with two distinct physical regions. Interior image points are employed at the boundary between the two regions. Matrix algebra is used to eliminate the interior image point coefficients so that BAND[16] may be used directly to obtain the solution. It was found that this method was not as accurate as the half-mesh-point formulation outlined here. Specifically, the interior-image-point formulation would calculate a small disappearance of total hydrogen at the salt film-solution interface when the current density was uniform over the entire distance domain. The half-mesh-point formulation balanced total hydrogen correctly at the interface.

Zero-time solution

Zero time is the instant when the ferrous sulfate first precipitates. The boundary conditions for the concentrations at ξ_{max} are taken as the values of the long concentration profiles at $x = 0$. The boundary conditions at the salt film-solution interface given by Equations (57) and (58) are programmed as stated in the text. Equation (59) requires modification at $t = 0$. Specifically, the left side of this equation is rewritten as

$$(1-\epsilon_f)D_4\rho_f\sqrt{t}\,\delta\frac{d(\sqrt{t}\,\delta)}{dt} = (1-\epsilon_f)D_4\rho_f\left(t\,\delta\frac{d\delta}{dt}+\frac{\delta^2}{2}\right). \tag{71}$$

At $t = 0$, boundary condition Equation (59) becomes

$$(1-\epsilon_f)D_4\rho_f\frac{\delta^2}{2} = N_4^{net}\,. \tag{72}$$

This equation is programmed in terms of the variable δ $(= \delta_x/\sqrt{t}\,)$, not the salt-film thickness itself.

The zero-time boundary conditions at the electrode surface are obtained from a perturbation analysis of the initial film-formation process.[26] The

perturbation results indicate that

$$\left.\frac{\partial c_i}{\partial \eta}\right|_{\eta=0} = 0\,; \quad i = 1 \text{ to } 4\,, \tag{73}$$

and

$$\left.\frac{\partial \Phi}{\partial \eta}\right|_{\eta=0} = 0\,. \tag{74}$$

These results may be rationalized by noting that the film has zero thickness at $t = t_{o+}$. The terms that explicitly contain t in Equations (41) and (42) are set equal to zero before these equations are linearized and solved. The governing equations for the salt film reduce to $c_i = constant$ and $\Phi = constant$ according to the perturbation results and the arguments presented above.

Perturbation approach to error analysis

As time increases from t_{o+}, the concentrations used for the boundary conditions at ξ_{max} are equated to the concentrations on the long concentration profiles at $x_{\xi_{max}}$ [see Equations (51) and (52) and Figure 5]. The long concentration profiles are frozen during this time-stepping process. This procedure results in an error in the calculation. As time increases, the actual long profiles will change in a transient manner. A perturbation analysis provides a method that permits these outer long profiles to change according to the governing transient differential equations. This analysis is presented by Russell;[26] however, the resulting equations were not numerically solved because of the excessive computation time involved.

If the long concentration profile of ferrous ions were uniform, and migrational effects were ignored, the salt-film thickness would be expected to be proportional to the square root of time. Deviations from this square-root dependence are expected because neither of these conditions is met. A full solution to the perturbation problem would result in a quantitative calculation of the deviations from the square-root-of-time salt-film growth

rate.

A further objective of this perturbation analysis is to calculate accurately the short-time current density just after initial salt-film formation. The details of this calculation are presented elsewhere,[26] but the results will be summarized in the next section. As noted in the previous section, the perturbation analysis also indicates the correct form for boundary conditions at $t = t_{o+}$. It is not necessary to carry out a full numerical solution of the perturbation problem in order to obtain the two results just described.

As t increases to values approaching unity, the position at $x_{\xi_{max}}$ will equal or exceed x_{max}. At this point the boundary conditions for the bulk solution, Equations (20) to (24) may be used at ξ_{max}. The location of the position corresponding to $x_{\xi_{max}}$ grows to distances exceeding the diffusion-layer thickness as $t \rightarrow 1$. At this time, there is no longer an error associated with the frozen long profiles because they are not used to set outer boundary conditions. The integrals in Equation (69) will vanish at this time, making this equation essentially equivalent to Equation (34).

Results

Zero-time profile

Figure 5 is a plot of the concentration profiles and the potential profile at $t = t_{o+}$. The portions of the abscissa corresponding to the variables η and ξ are greatly expanded in this plot. These two regions actually have a physical width of zero at $t = t_{o+}$. The potential profile at t_{o+} is calculated assuming that $\epsilon_s = 0.01$ at the instant of initial salt-film formation. The long profiles are unchanged from those at t_{o-} because no time has elapsed.

Change in current density

A decrease in superficial current density is expected with initial salt-film formation. Figure 8 is a plot of the superficial current density as a function of $(V - \Phi_o)$ for ϵ_s = 1.0, 0.1, and 0.01. The dashed line represents the ohmic limit. The intersection of the ohmic limit line with any of the three current-potential curves represents the superficial current density which would flow if varying conductivity in the diffusion layer and diffusion potentials were ignored.

During phase 1, no salt film covers the electrode surface, so that ϵ_s = 1.0. The superficial current density is equal to the Butler-Volmer current density. At t_{o-}, the superficial current density is 1.915 A/cm^2, as shown by point *A* on Figure 8. These results are calculated with the parameters listed in Table 1. Point A has a current density that is lower than the intersection of the ohmic limit curve with this current-potential curve. This decrease is due to the additional resistances associated with the two factors mentioned above. If the initial salt film forms with ϵ_s = 0.1, the superficial current density decreases to a numerically calculated value of 1.760 A/cm^2. The Butler-Volmer current density is a factor of $1/\epsilon_s$ (=10) higher than the superficial value. Therefore, the value of $(V - \Phi_o)$ increases to -0.0794 V from -0.1364 V to permit this higher current density. A similar, but more dramatic, effect is observed for ϵ_s = 0.01. The Butler-Volmer current density must now be 100 times larger than the superficial current density. $(V - \Phi_o)$ increases to -0.0228 V, and the superficial current density decreases to a numerically calculated value of 1.595 A/cm^2.

The current densities calculated by the program and plotted on Figure 8 are obtained at the end of the first time step following initial precipitation. The end of the first time step corresponds to a calculated time of 5.6x10^{-7} s after initial salt-film formation. To calculate a value of the current density at

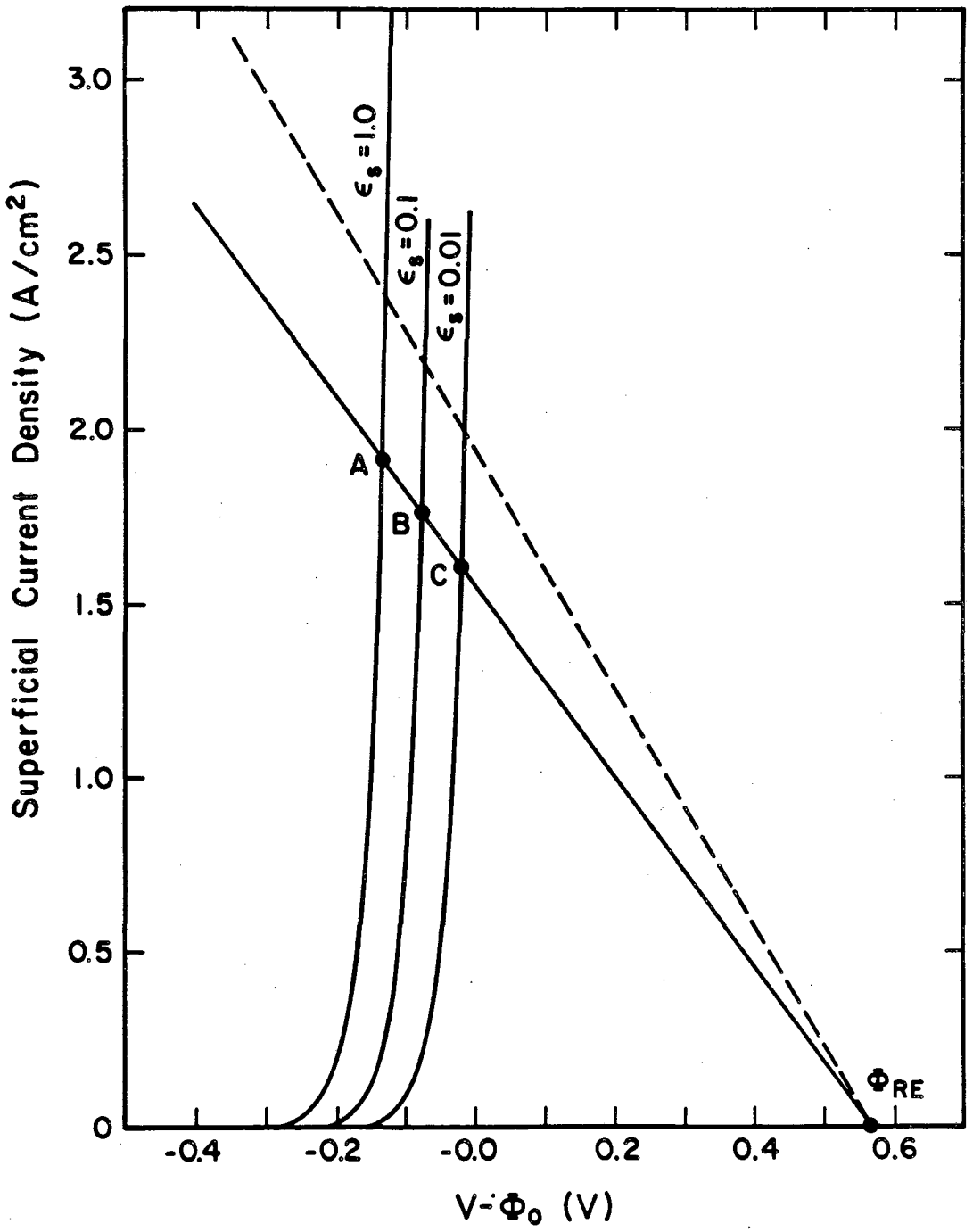

Figure 8. Superficial current density for three values of ϵ_s. Point A is the superficial current density for t_{o-}. Points B and C are the superficial current densities at t_{o+} for ϵ_s = 0.1 and 0.01, respectively.

initial formation, the perturbation approach must be used. The zero time current densities calculated from the perturbation equations are 1.758 A/cm^2 for $\epsilon_s = 0.1$ and 1.594 A/cm^2 for $\epsilon_s = 0.01$. The numerically calculated current density is within 0.12% of the perturbation result. This indicates that the computer simulation is accurately modeling the physical phenomena occurring near zero time.

The initial increase in salt-film thickness is nearly proportional to the square root of time. This is shown in Table 3, where it is seen that δ is nearly a constant function of the dimensionless time, t.

The small increase in δ observed at very short times is due to the flux of ferrous arriving through the pores of the salt film. This flux adds to the flux arriving from the electrolytic solution and allows the film to increase slightly more rapidly than it would if diffusion from solution were the only source of material for salt-film growth. At later times, the value of δ decreases noticeably. This is due to a reduction in the flux of material diffusing from the electrolytic solution. This reduction is caused by the decrease in the maximum concentration of ferrous ions in the electrolyte. At larger values of t, the concentration profile of ferrous ions will be a monotonically decreasing function in the electrolyte. Under these conditions the salt film will always dissolve into the electrolytic solution. The continued corrosion current provides a flux of material that is used to maintain the presence of the salt film. The increasing ferrous ion concentration at the electrode surface will increase the back reaction rate. The flux of ferrous ions moving through the salt film will decrease, and this will also cause δ to decrease.

Part II of this series[28] describes changes in potential and concentration profiles that occur in the pores of the salt film. These changes, along with changes in the surface porosity, are responsible for the oscillations observed in the iron-sulfuric acid system.

Table 3.

Values of t and δ during the initial stages of salt-film formation.

t	δ
0.000	0.3578
2.346×10^{-6}	0.3581
5.505×10^{-6}	0.3584
1.292×10^{-5}	0.3585
3.030×10^{-5}	0.3586
7.110×10^{-5}	0.3584
1.668×10^{-4}	0.3581
3.914×10^{-4}	0.3575
9.183×10^{-4}	0.3564
2.154×10^{-3}	0.3544
5.055×10^{-3}	0.3506
1.186×10^{-2}	0.3435
2.426×10^{-2}	0.3303
4.101×10^{-2}	0.3139
5.035×10^{-2}	0.3053

Acknowledgment

This work was partially supported by the Assistant Secretary of Conservation and Renewable Energy, Office of Energy Systems Research, Energy Storage Division of the United States Department of Energy under Contract Number DE-AC03-76SF00098. Equally important funding was received from the National Science Foundation under Grant No. CPE-8219827.

List of symbols

a	disk hydrodynamic constant, 0.51023
c_i	concentration of species i, mol/cm^3
D_i	diffusion coefficient for species i, cm^2/s
dt	time step size
F	Faraday's constant, 96,487 C/equiv
i	superficial current density, A/cm^2
i_{bv}	current density given by Butler-Volmer eq., A/cm^2
i_p	pore current density, A/cm^2
j	mesh point number
K	bisulfate-sulfate equilibrium constant, mol/cm^3
k_a	anodic rate constant, mol/cm^2-s
k_c	cathodic rate constant, cm/s
N	molar flux, mol/cm^2-s
N_i^f	reduced flux of species i in the salt film, mol/cm-s
N_i^s	reduced flux of species i in solution, mol/cm-s
N_i^{net}	reduced net flux at film-solution interface, mol/cm-s
N_i^{sur}	reduced flux at electrode surface, mol/cm-s
R	gas constant, 8.314 J/mol-K
R_i	rate of homogeneous reaction, mol/cm^3-s
r_o	radius of electrode, cm
s_i	stoichiometric coefficient
T	absolute temperature, K
t	dimensionless time
t^*	time, s
u_i	ionic mobility, cm^2-mol/J-s
V	electrode potential, V

v	velocity, cm/s
x	dimensionless distance from electrode
y	distance from electrode, cm
z_i	charge number

Greek letters

α_a	anodic transfer coefficient
α_c	cathodic transfer coefficient
δ	reduced salt-film thickness ($\delta_x/\sqrt{t}$)
δ_x	dimensionless salt-film thickness
δ_y	salt-film thickness, cm
ϵ_f	salt-film porosity
ϵ_s	surface porosity
η	reduced distance variable in the salt film
κ	conductivity, $(\Omega\text{-cm})^{-1}$
$\kappa_{H_2SO_4}$	conductivity of bulk solution, $(\Omega\text{-cm})^{-1}$
ν	kinematic viscosity, cm^2/s
ξ	stretched variable in the electrolytic solution
ρ_f	molar density of salt film, mol/cm^3
Φ	potential in solution, V
Φ_o	potential just outside diffuse double layer, V
Φ_{RE}	potential of a reference electrode of a given kind, V
Ψ	dimensionless overpotential
Ω	disk rotation speed, rad/s

subscripts

Hg/Hg_2SO_4	mercury-mercurous sulfate reference electrode
i	species i
o	position just outside the diffuse double layer

References

1. J. J. Podestá, R. C. V. Piatti, and A. J. Arvía. "The Potentiostatic Current Oscillations at Iron/Sulfuric Acid Solution Interfaces." *Journal of the Electrochemical Society*, **126** (1979), 1363-1367.

2. Philip Russell and John Newman. "Current Oscillations Observed within the Limiting-Current Plateau for Iron in Sulfuric Acid." Submitted to the *Journal of the Electrochemical Society*, 1985.

3. Theodore R. Beck. "Formation of Salt Films during the Passivation of Iron." *Journal of the Electrochemical Society*, **129** (1982), 2412-2418.

4. Richard Alkire, Daniel Ernsberger, and Theodore R. Beck. "Occurrence of Salt Films during Repassivation of Newly Generated Metal Surfaces." *Journal of the Electrochemical Society*, **125** (1978), 1382-1388.

5. Richard Alkire and Antonia Cangellari. "Formation of Salt Films during Anodic Metal Dissolution in the Presence of Fluid Flow." *Journal of the Electrochemical Society*, **130** (1983), 1252-1259.

6. John S. Newman. *Electrochemical Systems*. Englewood Cliffs, New Jersey: Prentice-Hall, Inc., 1973.

7. Limin Hsueh. *Diffusion and Migration in Electrochemical Systems*. Dissertation. Berkeley: University of California, 1968. (UCRL-18597 Rev., 1971)

8. Limin Hsueh and John Newman. "The Role of Bisulfate Ions in Ionic Migration Effects." *Industrial and Engineering Chemistry Fundamentals*, **10** (1971), 615-620.

9. W. G. Cochran. "The flow due to a rotating disc." *Proceedings of the Cambridge Philosophical Society*, **30** (1934), 365-375.

10. M. H. Rogers and G. N. Lance. "The rotationally symmetric flow of a viscous fluid in the presence of an infinite rotating disk." *Journal of Fluid*

Mechanics, **7** (1960), 617-631.

11. Kemal Nişancioğlu and John Newman. "Transient Convective Diffusion to a Disk Electrode." *Journal of Electroanalytical Chemistry and Interfacial Electrochemistry*, **50** (1974), 23-29.

12. John Newman. "Effect of Ionic Migration on Limiting Currents." *Industrial and Engineering Chemistry Fundamentals*, **5** (1966), 525-529.

13. Clarence G. Law, Jr., and John Newman. "A Model for the Anodic Dissolution of Iron in Sulfuric Acid." *Journal of the Electrochemical Society*, **126** (1979), 2150-2155.

14. J. O'M. Bockris, D. Drazic, and A. R. Despic. "The Electrode Kinetics of the Deposition and Dissolution of Iron." *Electrochimica Acta*, **4** (1961), 325-361.

15. John Newman. "Resistance for Flow of Current to a Disk." *Journal of the Electrochemical Society*, **113** (1966), 501-502.

16. John Newman. "Numerical Solution of Coupled, Ordinary Differential Equations." *Industrial and Engineering Chemistry Fundamentals*, **7** (1968), 514-517.

17. J. Crank and P. Nicholson. *Proceedings of the Cambridge Philosophical Society*, **43** (1947), 50.

18. Jadwiga Demichowicz-Pigoniowa. "Viscosity of Aqueous Solutions of $CdSO_4$." *Roczniki Chemii*, **33** (1959), 203-204.

19. W. Herz. "Die innere Reibung von Salzlösungen." *Zeitschrift für Anorganische Chemie*, **89** (1914), 393-396.

20. W. F. Linke. *Solubilities*. 1, Fourth Edition, New York: American Chemical Society, 1958.

21. B. G. Ateya and H. W. Pickering. "Effects of Mass Transfer in the Aqueous Phase on Repassivation of Activated Surfaces and the Stability of

Protective Films." *Passivity of Metals; Corrosion Monograph Series*. R. P. Frankenthal and J. Kruger, eds. Princeton, New Jersey: The Electrochemical Society, Inc., pp. 350-368.

22. William Tiedemann and John Newman. "Growing Porous Layers." *Journal of the Electrochemical Society*, **119** (1972), 186-188.

23. Richard Pollard. *Mathematical Modeling of the Lithium-Aluminum, Iron Sulfide Battery*. Dissertation. Berkeley: University of California, 1979. (LBL-10197)

24. Richard Pollard and John Newman. "Mathematical Modeling of the Lithium-Aluminum, Iron Sulfide Battery. I. Galvanostatic Discharge Behavior." *Journal of the Electrochemical Society*, **128** (1981), 491-502.

25. Richard Pollard and John Newman. "Mathematical Modeling of the Lithium-Aluminum, Iron Sulfide Battery. II. The Influence of Relaxation Time on the Charging Characteristics." *Journal of the Electrochemical Society*, **128** (1981), 503-507.

26. Philip Paul Russell. *Corrosion of Iron: The Active-Passive Transition and Sustained Electrochemical Oscillations*. Dissertation. Berkeley: University of California, June, 1984.

27. Ralph Edward White. *Simultaneous Reactions on a Rotating-Disk Electrode*. Dissertation. Berkeley: University of California, 1977. (LBL-6094)

28. Philip Russell and John Newman. "Anodic Dissolution of Iron in Acidic Sulfate Electrolytes. Part II. Mathematical Model of Current Oscillations Observed under Potentiostatic Conditions." Submitted to the *Journal of the Electrochemical Society*, 1985.

Figure Captions

Figure 1. The concentration profile of ferrous and hydrogen ions a short time after the beginning of precipitation.

Figure 2. Kinetic data obtained from a rotating hemispherical electrode in 1 M H_2SO_4. Temperature was 25±0.1°C.

Figure 3. Breakdown of $(V - \Phi_{RE})$ into a number of tractable components.

Figure 4. Speed of convergence is compared for the algebraic form and the logarithmic form of the Butler-Volmer equation.

Figure 5. Potential and concentration profiles at t_{o-} are shown for values on the abscissa of $0 < x < 5$. At t_{o-}, the electrode surface is located at $x = 0$. Potential and concentration profiles at t_{o+} in the salt film (abscissa variable η) and solution region described by the stretched variable ξ are included. The profiles on x are unchanged at t_{o+}.

Figure 6. Structure of the equations for the salt film-solution geometry. Boundary conditions are indicated by an open square.

Figure 7. Discretization of η and ξ for numerical computations.

Figure 8. Superficial current density for three values of ϵ_s. Point A is the superficial current density for t_{o-}. Points B and C are the superficial current densities at t_{o+} for $\epsilon_s = 0.1$ and 0.01, respectively.

This report was done with support from the Department of Energy. Any conclusions or opinions expressed in this report represent solely those of the author(s) and not necessarily those of The Regents of the University of California, the Lawrence Berkeley Laboratory or the Department of Energy.

Reference to a company or product name does not imply approval or recommendation of the product by the University of California or the U.S. Department of Energy to the exclusion of others that may be suitable.

LAWRENCE BERKELEY LABORATORY
TECHNICAL INFORMATION DEPARTMENT
UNIVERSITY OF CALIFORNIA
BERKELEY, CALIFORNIA 94720